SE8700091

ISSN 0348-7539

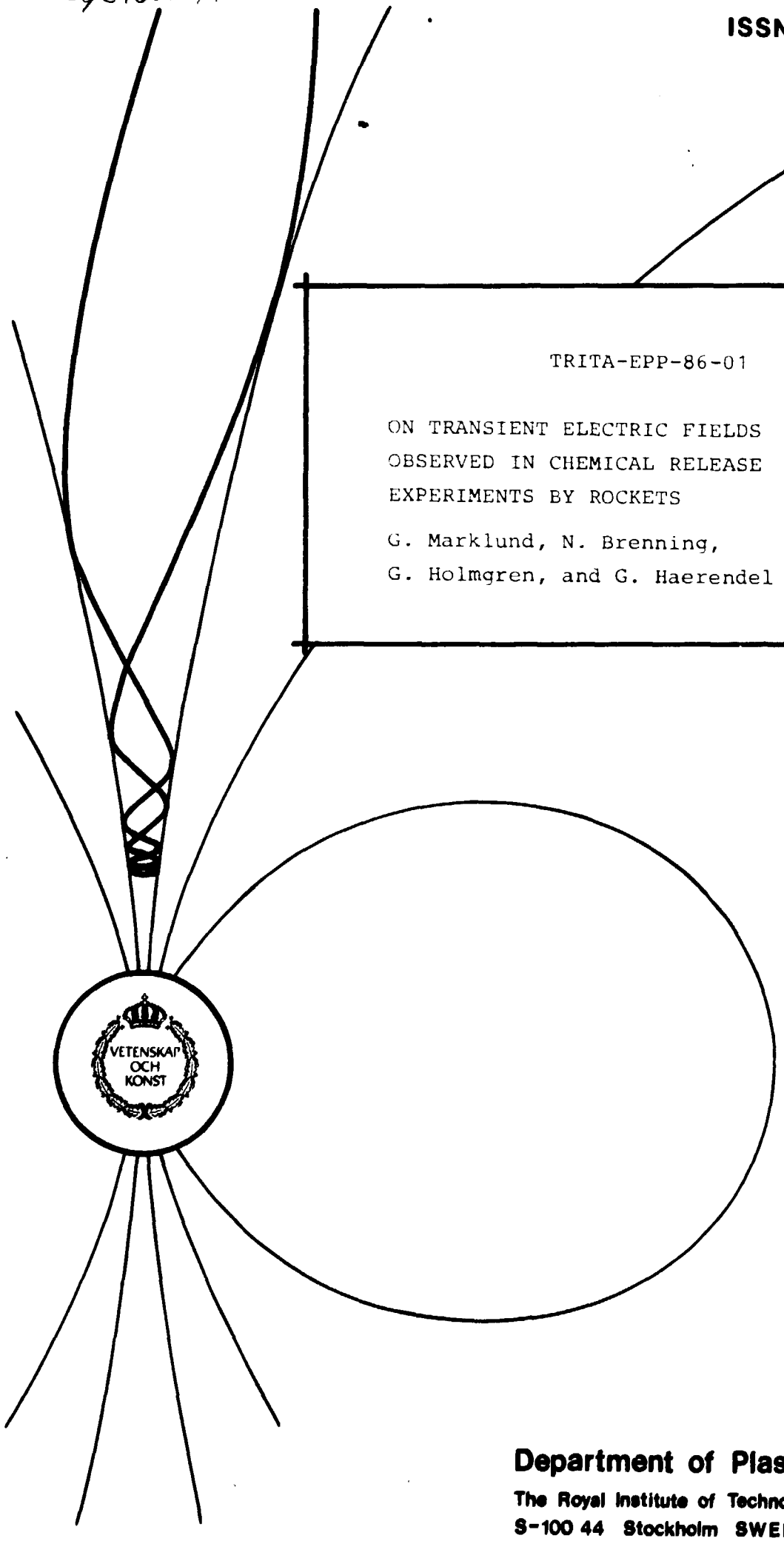

TRITA-EPP-86-01

ON TRANSIENT ELECTRIC FIELDS OBSERVED IN CHEMICAL RELEASE EXPERIMENTS BY ROCKETS

G. Marklund, N. Brenning,
G. Holmgren, and G. Haerendel

Department of Plasma Physics
The Royal Institute of Technology
S-100 44 Stockholm SWEDEN

TRITA-EPP-86-01

ON TRANSIENT ELECTRIC FIELDS OBSERVED IN CHEMICAL RELEASE EXPERIMENTS BY ROCKETS

G. Marklund, N. Brenning,
G. Holmgren, and G. Haerendel

June 1986

Department of Plasma Physics
The Royal Institute of Technology
S-100 44 Stockholm, Sweden

ON TRANSIENT ELECTRIC FIELDS OBSERVED IN CHEMICAL RELEASE EXPERIMENTS BY ROCKETS

G. Marklund[1], N. Brenning[1], G. Holmgren[2] and G. Haerendel[3]

(1) Dept of Plasma Physics, The Royal Institute of Technology, S-100 44 Stockholm, Sweden
(2) Uppsala Ionospheric Observatory, S-755 90 Uppsala, Sweden
(3) Max-Planck-Institut für extraterrestrische Physik, D-8040 Garching bei München, BRD

Abstract

As a follow-up to the successful chemical release experiment Trigger in 1977, the TOR (Trigger Optimized Repetition) rocket was launched from Esrange on Oct. 24, 1984. Like in the Trigger experiment a large amplitude electric field pulse of 200 mV/m was detected shortly after the explosion. The central part of the pulse was found to be clearly correlated with an intense layer of swept up ambient particles behind a propagating shock-front. The field was directed towards the centre of the expanding ionized cloud, which is indicative of a polarisation electric field source. Expressions for this radial polarisation field and the much weaker azimuthal induced electric field are derived from a simple cylindrical model for the field and the expanding neutral cloud. Time profiles of the radial electric field are shown to be in good agreement with observations.

1. Introduction

In this paper we present a simple but useful model to describe the intense transient electric field pulses that have been observed in connection with chemical release experiments by rockets in the auroral ionosphere. We will here primarily focus on the results from the release experiment on the TOR (Trigger Optimized Repetition) rocket, launched from Esrange on October 24, 1984. Comparisons will however also be made with results from an earlier and similar experiment on the Trigger rocket launched from Esrange on February 11, 1977. Both these experiments used Cs-doped high explosives that are described in more detail in Appendix 1. The Trigger observations have been reported earlier in e.g. Holmgren et al. (1980), Kelley et al. (1980) and Lundin and Holmgren (1980). The geometry of the TOR and Trigger experiments are schematically pictured in Fig. 1. We will here concentrate on the upper of the TOR releases and the Trigger release, which were both made at about the same altitudes (≈ 170 km) and for similar ionospheric conditions.

2. Observations

In Fig. 2 the TOR electric field data are summarized in a vector representation. The upper panel shows the ambient ionospheric electric field vs flight time and the lower panel the electric field associated with the explosion vs time after the explosion (note the expanded timescale). The ambient field has a stable orientation towards north-northeast and increased in magnitude from 10 mV/m in the beginning of the flight to 20 mV/m at the end of the flight.

The electric field inferred from the STARE-drift observations (by courtesy of E. Nielsen) and indicated by the thick arrow, agrees well with the rocket data. The Esrange magnetometer data also indicates the presence of a weak eastward electrojet at this time (data not shown here) in good agreement with the observed northward electric field. A description of the other observations made on the TOR rocket and from the ground will be

given elsewhere (Holmgren et al., 1986).

Thanks to the stable ionospheric conditions that prevailed in the rocket area at the time around the explosion, the electric field directly generated by the release is clearly distinguishable from the background field as demonstrated in the lower panel. A few milliseconds after the explosion the field reversed from the ambient northward field to a predominantly southward field, which increased to a maximum value of 240 mV/m within 60 ms. The duration of the pulse was roughly 250 ms. The direction towards the cloud centre, indicated by the thick arrow, fits well with the average direction of the pulse.

The electric field data from the Trigger experiment have been presented and discussed in Kelley et al. (1980). In Fig.3 the dominant northward component of the electric field associated with the Trigger release is shown versus time after the explosion together with some other profiles that will be discussed below. The daughter separation was here forward (cf. Fig. 1) such that the direction from the rocket to the cloud centre in a plane perpendicular to $\underline{B}$ became roughly northward. The field started to increase 10 ms after the explosion and a broad peak of 95 mV/m was observed at 105 ms followed by a more narrow peak of 180 mV/m at 135 ms. The duration of the pulse was also here about 250 ms. The ambient field was typically smaller than 10 mV/m.

To summarize, in two similar but separate release experiments transient electric field pulses with similar characteristics were observed shortly after the explosion. The pulses peaked between 0.06-0.15 after the explosions with maxima of about 100-250 mV/m, lasted for about 0.25 s and were oriented roughly towards the centre of the expanding clouds. The radial direction of the field towards the cloud centre is suggestive of a radial polarisation field source.

3. Neutral cloud model

The transient phenomena that we will focus on here occurred within less than 300 milliseconds after the release. The neutral cloud expansion is essentially gas dynamical in nature, i.e., very little influenced by the motion of the plasma component and by the magnetic field. A spherical shock front travels outwards and sweeps up the ambient material. Within a few mean free paths behind the shock front, the swept-up ambient particles dominate the cloud composition, and the velocity and density are given by the shock equations. Further in, towards the center of the explosion, the neutral gas and plasma compositions gradually change to those of the expanding cloud, and the neutral velocity and density approach those of a neutral cloud expanding in vacuum.

The magnetic field line on which the rocket is situated will be swept over by these different parts of the neutral cloud in a time sequence. We will here use a cylindrical model for the neutral cloud, originally intended to describe the free expansion of a cloud into vacuum. With some modifications this model can be used also to approximate the situation behind the shock front; this will be discussed further in section 5.

The model is illustrated in Fig.4. The density of the neutral gas cloud is taken to be zero for distances along B greater than $\pm$ $\Delta H/2$, while the density inside this limit is independent of z and given by a cut through the center of a spherical Gaussian distribution.

$$n_n(r,t) = N_n (t\, v_{ex})^{-3}\ \pi^{-3/2} \exp\{-r^2/(t\, v_{ex})^2\} \qquad (1)$$

Here N_n is the total number of neutral particles, t is the time after the explosion, v_{ex} is the characteristic expansion velocity and r the radial distance from the cloud centre. ΔH is chosen so that the total number of neutral particles is the

same in the cylindrical model as the spherical Gaussian model would give. From this follows that $\Delta H = \sqrt{\pi} \cdot V_{ex} \cdot t$. During the initial phase the expansion velocity much exceeds both the rocket velocity transverse to $\underline{B}$ and the relative velocity between the rocket and the cloud. The rocket can thus be regarded as being fixed in space relative to the centre of the neutral cloud. Eq. (1) will here be used to calculate the time variation of the neutral gas density at the radial distance r_o, which is the distance between the field lines passing through the cloud centre and the rocket, as shown by Fig. 4.

4. Electric field and current model

The dynamics of the plasma cloud is very different from that of the neutral cloud. In fact the radial expansion of the electrons will essentially cease as soon as the mean free path for electron-neutral collisions exceeds the electron gyroradius. The ions will due to their larger iongyroradia be further pushed outwards by the neutrals but the charge separation that develops results in a radially inward polarisation electric field. This field will increase until it stops the ion expansion unless the positive charge can be neutralized by Birkeland currents.

Consider a cylindrical coordinate system to describe the electric field and the current flow within the cloud. A steady state conductivity concept will be used since, for the initial phase of expansion studied here, the characteristic time scale for electric field variations ($\tau \approx 0.1$ s) exceeds the time between ion-neutral collisions ($\nu_{in}^{-1} \approx 0.01$ s) (see Section 7).

The radial and azimuthal currents are given by:

$$\begin{pmatrix} j_r \\ j_\varphi \end{pmatrix} = \begin{pmatrix} E_r \, , & E_\varphi + V_n B \\ E_\varphi + V_n B \, , & -E_r \end{pmatrix} \begin{pmatrix} \sigma_p \\ \sigma_H \end{pmatrix} \qquad (2)$$

$$(3)$$

We have here assumed an azimuthal symmetry and an essentially unchanged magnetic field at the distance r_o from the centre of the cloud. The latter assumption will be justified a posteriori (Appendix 2). E_r and E_φ denote the radial polarisation electric field and azimuthal induced electric field, v_n the neutral gas velocity, and σ_P and σ_H the Pedersen and Hall conductivities.

Two things are needed to complete the system of Equations (2) and (3).

(1) A relationship between $j_\parallel$ (drawn from the surrounding plasma) and the electric field generated in the cloud.

(2) The relationship between E_φ and j_φ given by Maxwell's equations. This requires some additional assumptions about E_φ and j_φ, e.g. about the radial profile.

Fortunately, for both the TOR and Trigger experiments, $j_\parallel$ and j_φ only have relatively small influence on the electric field, which is the parameter of prime interest here. In Appendix 2 it is shown that E_φ is much smaller than both E_r and V_nB, since the magnetic Reynolds number $R_m = DV\mu_o\sigma_p << 1$.

It is also clear from the observations that the electric fields were essentially radial (cf. Fig.2).

Thus Eqs.(2) and (3) reduce to

$$\begin{pmatrix} j_r \\ j_\varphi \end{pmatrix} = \begin{pmatrix} E_r & V_nB \\ V_nB & -E_r \end{pmatrix} \begin{pmatrix} \sigma_p \\ \sigma_H \end{pmatrix} \qquad (4)$$

$$(5)$$

The general expressions which apply when the criteria $E_\varphi << E_r$ is not fulfilled, are given in Appendix 2.

The radial current described by Eq.(4) is composed of two terms: the Hall current driven by the neutral gas and the opposing Pedersen current driven by the polarisation electric field. The residual ion current j_r has to be closed by field-

-aligned currents, $j_{\parallel}$. A relation between j_r and $j_{\parallel}$ can be obtained from

$$\text{div } \underset{\sim}{j} = 0 \tag{6}$$

which in cylindrical geometry can be expressed as

$$\frac{1}{r}\frac{\partial}{\partial r}(rJ_r) + \frac{1}{r}\frac{\partial j\varphi}{\partial \varphi} + \frac{\partial jz}{\partial z} = 0 \tag{7}$$

The middle term vanishes due to the cylindrical symmetry and the remaining equation becomes after being height-integrated over ΔH,

$$\frac{1}{r}\frac{\partial}{\partial r}(rJ_r) = -\int_{-\Delta H/2}^{+\Delta H/2} \frac{\partial jz}{\partial z}\, dz \tag{8}$$

where J_r and $\Sigma_{P(H)}$ are defined by

$$J_r = \Sigma_P E_r + \Sigma_H V_n B \tag{9}$$

$$\Sigma_{P(H)} = -\int_{-\Delta H/2}^{+\Delta H/2} \sigma_{p(H)}\, dz \tag{10}$$

Using Eq.(9) and the following assumption based on the cloud symmetry (cf. Fig.4)

$$j_z(+\Delta H/2) \approx -j_z(-\Delta H/2) \tag{11}$$

Eq.(8) can be rewritten as

$$\frac{1}{r}\frac{\partial}{\partial r}[r(\Sigma_P E_r + \Sigma_H V_n B)] = -2j_z(+\Delta H/2) \tag{12}$$

The magnitude of j_z can be estimated from a relation between the field-aligned current and transverse wave electric field in an Alfvén wave as given by Carlsson and Kelley (1977), Mallincrodt and Carlsson (1978)

$$j_z = \Sigma_A \text{div } \underset{\sim}{E_\perp} \tag{13}$$

Here Σ_A represents the Alfvén wave conductance defined by

$$\Sigma_A = \frac{1}{\mu_o V_A}$$

where V_A is the Alfvén wave velocity. Eqs.(12) and (13) give

$$\frac{\partial}{\partial r}\left[r(\Sigma_P E_r + \Sigma_H V_n B)\right] = -2\Sigma_A \frac{\partial}{\partial r}\left[rE_r\right] \qquad (14)$$

The relative influence of the right hand side of this equation is roughly given by the ratio Σ_A/Σ_P. As shown in Appendix 3, this ratio for the TOR and Trigger experiments depends on the assumed form of the expansion for the ion cloud. A spherical expansion gives about 0.2 and a cylindrical expansion 0.8. It is therefore not clear from the observations that Σ_A/Σ_P is so small that the right-hand term in Eq.(14) can be neglected. However, we here assume this to be the case, i.e. that the polarisation field E_r is mainly determined by the balance between the Hall current and opposing Pedersen current:

$$E_r \approx -\frac{\Sigma_H}{\Sigma_P} V_n B \qquad (15)$$

The modification of this result due to Birkeland currents may be roughly estimated by comparing the different terms in Eq.(12). We now have

$$E_r \approx -\frac{\Sigma_H}{\Sigma_P + 2\Sigma_A} V_n B = -\frac{\Sigma_H}{\Sigma_P} V_n B \cdot \beta \qquad (16)$$

Here β, as defined by

$$\beta = \left(1 + \frac{2\Sigma_A}{\Sigma_P}\right)^{-1} \qquad (17)$$

can be thought of as a reduction factor for the radial polarisation electric field (from the value given by Eq.(15)) due to Birkeland currents. For the derived Σ_A/Σ_P-ratios (cf. Appendix 3), β will assume a value between 0.7 and 0.4. Let us return to Eq.(15). Since we are in the parameter range where $\nu_{en}/\omega_{ce} \ll 1$ the Σ_H/Σ_P-ratio is essentially equal to the ratio between the ion-neutral collision frequency and the

ion-gyro frequency, i.e. ν_{in}/ω_{ci}. Thus Eq. (15) for E_r can be expressed as

$$E_r = - \frac{\nu_{in}}{\omega_{ci}} V_n B \tag{18}$$

To calculate the electric fields presented in the next section we use the following expressions for the various terms in Eq.(18) .

$$\nu_{in} = k \cdot n_n \tag{19}$$

where k is the collision rate coefficient and n_n the neutral gas density calculated at r_o, using Eq.(1) above. The average ion gyro frequency in the cloud is given by

$$\omega_{ci} = \frac{eB}{\langle m_i \rangle} \tag{20}$$

where $\langle m_i \rangle$ represents the average ion mass. k and ω_{ci} will attain different values in different regions of the expanding cloud as will be discussed in the next section. The neutral gas velocity is calculated from

$$V_n = \frac{r_o}{t} \tag{21}$$

Eqs.(1) and (18)-(21) gives an analytical expression for E_r which attains a maximum given by:

$$E_r^m = \frac{4}{\pi^{3/2} \exp(2)} \cdot \frac{k \cdot N_n \langle m_i \rangle V_{ex}}{e\, r_o^3} \tag{22}$$

at the time

$$t^m = \frac{1}{\sqrt{2}} \frac{r_o}{v_{ex}} \tag{23}$$

Thus the magnitude of the pulse is proportional to the collision rate coefficient k, the total number of neutral particles in the cloud, the average ion mass, the characteristic expansion velocity of the neutrals and inversely proportional to the cube of the radial distance r_o.
Since r_o is known, we can obtain an estimate of v_{ex} from the observed time of the peak, t^o:

$$v_{ex} = \frac{1}{\sqrt{2}} \frac{r_o}{t^o} \tag{24}$$

5. Validity of the model

Eqs. (18) and (19) give the following expression for the radial electric field:

$$E_r = - \sigma v_{rel} n_n v_n B/\omega_{ci} \tag{25}$$

where the collision rate coefficient k has been written out as σv_{rel}, i.e. the product of the cross-section and the relative velocity between ions and neutrals. This expression is not limited to any particular neutral gas model, but is applicable in the whole expanding cloud provided that the following conditions which have been discussed above are valid, namely: $DV_n \mu_o \sigma_p << 1$ (App.2); steady state conductivity concept ($\tau >> \nu_{in}^{-1}$, see Section 7); and $\Sigma_A << \Sigma_p$ (App.3).

It is practical for this discussion to split up the factors in Eq. (25) into $n_n v_n$, v_{rel}, and σ/ω_{ci} since these parameters will change in a fairly predictable way in the expanding cloud.

1. The product $n_n v_n$:

In the freely expanding cloud model referred to above this product is given by Eqs. (1) and (21) with v_{ex} given by Eq.

(24). A more realistic value close to the shock front can be obtained from classical theory of strong shocks. The equations presented below have been taken from Landau and Lifshitz (1959). The radial distance covered by a spherical shock front at a time t after the explosion is given by

$$r_s = \left(\frac{E_o}{\varrho_o}\right)^{\frac{1}{5}} \cdot t^{\frac{2}{5}} \qquad (26)$$

where E_o is the energy content of the explosive and ϱ_o the ambient mass density.

In an idealized strong shock where the mean free path $\lambda \ll r_s$, the particles immediately behind the shock front has the velocity

$$v_n = \frac{2}{\gamma+1} \cdot \dot{r}_s \qquad (27)$$

and the density

$$n_n = \frac{\gamma+1}{\gamma-1} \cdot n_o \qquad (28)$$

where γ is the ratio of specific heats c_p/c_v.

Some parameters for the shock model and for the freely expanding cloud model are given in Table 1 for TOR and Trigger, for the time of the maximum of the electric field. We find that the derived distances r_o, corresponding to the electric field maximum lies approximately four to five mean free paths inside the position of the idealized shock front. This is to be expected, since the electric field will have a maximum very close to the position where n_n has a maximum and the shock will require a few mean free paths to sweep up the ambient neutrals. Notice that the two models give close to the same value of $n_n v_n$, both for Tor and Trigger. A physical reason for this is that the freely expanding cloud underestimates n_n and overestimates v_n behind the shock, where a lot of ambient

material has been swept up. Due to the conservation of momentum, these two effects crudely balance each other.

Thus the freely expanding cloud model, which of course best describes the central part of the cloud, also gives a good approximation of the product $n_n v_n$ immediately behind the shock. We will therefore use this value of $n_n v_n$ in the whole expanding cloud. There is an important distinction here: we do not claim that Eq.(1) gives a representative value of n_n, or that Eq.(21) gives a representative value of v_n throughout the neutral cloud.

2. V_{rel}

The next parameter in Eq.(25), V_{rel}, immediately illustrates this distinction. Fig. 5 illustrates schematically the radial density variation in the TOR explosion that is expected from our combination of the freely expanding cloud and the shock model. In the central part of the cloud where the cloud is still freely expanding, v_n is well described by Eq.(21). In the region behind the shock front dominated by swept up ambient material v_n is more accurately described by Eq.(27). In our model with $\beta = 1$, $V_{rel} = v_n$.

3. σ/ω_{ci}

The last parameter in Eq.(25), σ/ω_{ci}, is determined by the ion species. These will gradually change from predominantly Cs^+ ions in the central part of the cloud to ambient ions such as NO^+, O_2^+ and O^+, immediately behind the shock front.

The cross section used for the collisions between the swept up ambient ions and neutrals is taken from Rees and Walker, 1968

$$\sigma \approx 1.07 \times 10^{-18} \cdot \left(1 + \frac{m_i}{m_n}\right)^{-1} \qquad (29)$$

According to Jones and Rees (1972) the average ion and neutral mass around 170 km altitude is 30 m.u. and 25 m.u. respectively. This gives

$$\sigma \approx 4.86 \cdot 10^{-19}\ m^2 \qquad (30)$$

$$\omega_{ci} \approx 160\ \text{rad/s} \qquad (31)$$

In the cloud plasma the main collisional processes are resonant charge exchange between Cs^+ and neutral Cs and collisions between Cs^+ and non-Cesium particles as listed in Appendix 1.

In spite of the small admixture of Cesium in the neutral cloud (4.7%, cf. Appendix 1) the large cross section $\sigma \approx 6 \cdot 10^{-18}$ m^2 (Andersen et al., 1972) makes the former collision important. The cross-section for Cs^+- non Cesium particles is estimated from Eq.(29) using $\langle m_i \rangle \approx 133$ m.u. and $\langle m_n \rangle = 24$ m.u. (cf. Appendix I). From the above, an effective cross-section representative for the cloud plasma can be estimated.

$$\sigma^{cloud} = \sigma_{Cs^+ - Cs} + \sigma_{Cs^+ - \text{non Cs}} \approx 4.4 \times 10^{-19}\ m^2 \qquad (32)$$

$$\omega_{ci}^{cloud} \approx 36.2\ \text{rad/s} \qquad (33)$$

Comparing Eqs.(30) and (31) representative for the shock region (ambient plasma) and Eqs.(32) and (33) representative for the cloud plasma one notes that the main difference in σ/ω_{ci} lies in the difference in ω_{ci} since σ is practically the same in both regions.

To summarize, three parameters have to be chosen to calculate the time profile of the electric field at r_o using Eq.(25). We consider it likely that the cloud can be roughly split up in three regions as illustrated in Fig.6. It is beyond the scope of this work to discuss how the transition goes from I to II to III as the cloud sweeps past the rocket field line in TOR and Trigger. Instead we have in Figs.7 and 3 presented the observa-

tions and superimposed theoretical curves labelled I, II and III according to the different parameters that have been put into Eq.(25). Since the limits between the various regions are somewhat uncertain we have indicated by solid and dashed lines where the results are believed to be reliable and less reliable respectively.

6. Results

Fig. 7 shows the southward component of the electric field observed on TOR (thick line) together with model profiles labelled I, II and III corresponding to the three different cloud regions illustrated in Fig. 6 and calculated using Eq. (25) with $\beta = 1$. The input parameter values that have been used are listed in Table 2. Model profiles I and II agree very well with the observed field, both in terms of the pulse magnitude and its general shape. An estimate of the peak value using Eq.(25) with n_n and v_n directly from the shock equations is denoted by a cross. Note that the pulse magnitude turns out to be almost the same using our model and the shock model. There is a plateau in the observed field around 120 ms which is here suggested to represent the transition between region 1 and region 2 (cf. Fig. 6). Profile III is calculated for the central parts of the expanding cloud (Region III).Since this corresponds to the end of the pulse, where the observed field approaches the ambient field value, a good agreement is not to be expected.

The model profiles calculated for the Trigger release is presented in the same way in Fig. 3. The input parameter values used are listed in Table 2. Profile I agrees very well with the large scale features of the pulse, both in terms of magnitude and shape although the observed field is rather fluctuating. In comparison with the TOR pulse, the Trigger pulse peaked later (at t = 105 ms for the broad maximum) due to the larger distance r_o, resulting in a wider pulse with smaller amplitude. This difference is illustrated also in Fig. 5, drawn for the TOR release, but representative also for the Trigger re-

lease. At t ≈ 120 ms, the particle layer behind the shock front is wider and less intense than for t = 60 ms. This is also consistent with a possible overestimation of E_{max} using the shock model as indicated by the cross in Fig.3. Due to the rapid deceleration and widening of the region behind the shock front, not much of Region II and III will be encountered at r_o within the lifetime of the pulse. At the end between 250 and 300 ms the model profile II agrees relatively well with the observed field.

To summarize, the agreement between the model and observed fields on TOR and Trigger is surprisingly good in terms of pulse amplitude and general shape. Note that the only adjustment of the model parameters listed in Table 2 that has been made is that the times between the observed and calculated field maxima have been put equal according to Eq. (24).

7. Discussion

The ionosphere plays in several respects an active role during magnetic substorms. This has been confirmed both from observations and theoretically. A well known ionospheric generator mechanism is the drag of ions transverse to B by neutral winds. Another generator mechanism is associated with the current closure across auroral forms, such as e.g. the current balance maintained within breakup auroras between the enhanced Hall current and the opposing Pedersen current driven by a polarisation electric field. The latter mechanism is however always accompanied by an external (magnetospheric) generator mechanism (cf. Marklund et al. 1985).

Chemical releases in the ionosphere, as examplified here by the TOR and Trigger releases, enable controlled studies of this problem. The rapidly expanding neutral cloud and the associated ion cloud together form a localized ionospheric generator which may, as shown by the Trigger results (Holmgren et al. 1980, Kelley et al. 1980), drive currents unstable to stimulate auro-

ral precipitation. The artificial generators studied here were found to be characterized by intense (≈250 mS) polarisation electric fields oriented towards the centre of the expanding clouds as demonstrated by the TOR pulse in Fig. 2 and the Trigger pulse in Fig. 3. The generator current can be seen as an outward Hall current driven by the neutral wind which here is partly cancelled by an inwards Pedersen current driven by the polarisation or generator field (cf. Eq.4). These oppositely directed currents are therefore both relatively large as compared to the net current j_r which has to close by field-aligned currents. The latter may however still have current densities comparable with those typical for natural aurora.

A rough measure of the relative influence on the radial current balance by Birkeland currents as compared to polarisation (i.e. right-hand term to any of the left-hand terms in Eq.12) is given by the ratio Σ_A/Σ_P, as discussed by Carlsson and Kelley (1977). For the ambient plasma densities prevailing during the TOR and Trigger experiments Σ_A = 0.5 S. Estimates of Σ_P integrated over the cloud range between 0.6 S and 2.6 S, depending on the assumed form of the ion cloud expansion (cf. Appendix 3). For the derived values of Σ_A/Σ_P 0.2 and 0.8 the reduction factor β, as defined by Eq.(17) lies in the range 0.7 to 0.4. This would correspond to measured electric fields 30 to 60% <u>below</u> the model fields, which have been calculated assuming negligible Birkeland currents (β = 1). Since we instead have a good agreement between the theoretical and experimental curves (cf. Figs.3 and 7) a β-value closer to 1 seems to be justified. Note in particular that the TOR and Trigger pulses of 240 mV/m and 100 mV/m (narrow peak 180 mV/m) are comparable with the corresponding V_nB-values of 180 and 130 mV/m as calculated using Eq.(27).

The β-factor was here derived by equating the divergence of j_r using a steady state description with an expression for $j_\parallel$ valid for a transient phenomena such as an Alfvén wave. The roughness in this procedure is here excused by the fact

that the $j_{\parallel}$-term is shown to effect the result only marginally. The expression for β should therefore not be interpreted too strictly but instead viewed as an attempt to estimate quantitatively the relative influence by Birkeland currents on the radial current balance within the cloud.

From the above discussion we may conclude that the radial field E_r seems to be dominated by the Hall and Pedersen current balance described by the simple equation (18) or equivalently that the influence on E_r by Birkeland currents seems to be small. A β-value close to 1 has a number of interesting implications for the cloud dynamics. First, the expanding cloud seems to act as a voltage generator where the generator field is primarily determined by the neutral gas density and expansion velocity and rather independent of the ion density and motion:

$$E_r = - (\frac{\nu_{in}}{\omega_i}) v_n B \qquad (18)$$

Secondly, the transverse expansion of the ions in the cloud is much reduced as compared to the neutral cloud expansion. The fraction of ions that leak through the radial voltage barrier is determined by the ionospheric current response to this generator. Since the electrons are trapped close to the center of the cloud, the radial ion currents are limited to what can be neutralized by field-aligned currents.

Finally, these results apply to two specific releases. In a situation where the plasma density within the cloud is lower, such that e.g. $\Sigma_P < \Sigma_A$, the generator field would have been much reduced (by more than 70%) and thus the influence by field-aligned currents on the radial current balance correspondingly large.

Thus, the intensity of the transient electric field pulses that will be generated in a release will depend on the ratio Σ_A/Σ_P, a parameter which depends strongly (through Σ_P) on the ion density in the cloud.

For $\Gamma_A/\Gamma_p < 1$ intense fields are to be expected
For $\Gamma_A/\Gamma_p > 1$ weak fields are to be expected

A rather unexpected result of these analysis presented here is that the central part of the observed electric field pulses seems to be dominated by the ambient plasma and not the cloud plasma. At the time these particles, swept up a few mean free paths behind the shock front, pass the field line connected with the rocket (r_o), the electric field peak is observed on the rocket. This is clearly confirmed by the excellent consistency between the geometrically derived r_o and the theoretically derived radius of the shock front $r_s(t^o)$ (using Eq.(26)) as seen in Table 1 and Fig.5. Due to the high neutral density behind the shock front (as given by Eq.(28)) which is to be associated with the main electric field peak, ν_{in} will assume rather large values in this region, typically 150-200 s^{-1}. This is comparable with the typical ambient ion gyro frequency of 160 rad/s. The use of the steady state conductivity concept which has been made here is thus justified since the characteristic time scale for electric field variations ($\tau \approx 0.1$ s) is an order of magnitude larger than the typical time between collisions and the gyro period ($\nu_{in}^{-1} \approx \omega_{ci}^{-1} \approx 0.01$ s).

7. Summary and Conclusions

A useful and simple model has been derived to describe the dynamics of expanding clouds released in the ionosphere during the initial phase of expansion which for the cases studied here corresponds to $t<0.3$ s. In particular the model is used to describe the transient electric fields that have been observed during the TOR and Trigger release experiments. The main findings are summarized below.

(1) The transient electric fields observed on Tor and Trigger were characterized by intense peaks between 100 and 250 mV/m, life times of 250 ms, essentially radial orientations towards the cloud centre. The azimuthal component

(induced field) was accordingly small. These main features are all well described by the model results.

(2) The central parts of the electric field peaks are found to be clearly correlated with the intense particle layer of swept up ambient plasma, a few mean free paths behind the shock front.

(3) The radial - or generator field E_r - is dominated by the balance between the outward Hall current, driven by V_n and the Pedersen current, driven by E_r. The relative influence on the generator field by $j_\parallel$ is relatively small, as here represented by a reduction factor β close to 1. The expanding cloud therefore acts essentially as a voltage generator.

(4) The electrons are trapped on the magnetic field lines close to the explosion, and the transverse expansion of the ions is much reduced as compared to that of the neutrals. The ion current that leaks through the generator voltage barrier is limited to the amount that can be closed by $j_\parallel$.

(5) The intensity of the transient electric fields that is generated in a release depends sensitively on the ratio Σ_A/Σ_p, which in turn depends strongly on the ion density in the cloud. The conclusions made above (1)-(3) hold for Σ_A/Σ_p small. In a situation where $\Sigma_A/\Sigma_p > 1$, the generator field will be relatively small and much of the outward Hall current can be closed by $j_\parallel$.

Acknowledgements

The authors are grateful to C.-G. Fälthanmmar and L. Block, The Royal Institute of Technology, C.W. Carlson, Space Sciences Laboratory, Berkeley, M.C. Kelley, Cornell University, Ithaca and

C.K. Goertz, University of Iowa for helpful comments and stimulating ideas, H. Föppl, Max-Planck-Institut für Extraterrestrische Physik, Garching, N. Hörnqvist and S.E. Flygar at the Research Institute for National Defense, Sweden, for providing essential information on the explosives and on the dynamics and composition of the produced clouds and E. Nielsen, Max-Planck--Institut für Aeronomie, Lindau, for providing the STARE data. Finally much thanks to E. Florman and K. Vikbladh for typing the manuscript and to K. Forsberg for the excellent drawings. This research was supported by the Swedish Board of Space Activities.

References

Andersen, S.A., Jensen, V.O., and Michelsen, P., 1972: Charge Exchange Cross Sections Measured at Low Energies in Q-Machines, Rev. Sci. Instr., 43, 945.

Boström, R., 1974: Ionosphere-Magnetosphere Coupling, in Magnetospheric Physics, Ed. B.M. McCormac, pp. 45-59, D. Reidel, Hingham, Mass., 1974.

Carlson, C.W. and Kelley, M.C., 1977: Observation and Interpretation of Particle and Electric Field Measurements Inside and Adjacent to an Active Auroral Arc., J. Geophys. Res., 82, 2349.

Evans, D.S., Maynard, N.C., Trøim, J., Jacobsen, T., and Egeland, A., 1977: Auroral Vector Electric Field and Particle Comparisons, 2, Electrodynamics of an Arc, J. Geophys. Res., 82, 2235.

Holmgren, G., Boström, R., Kelley, M.C., Kintner, P.M., Lundin, R., Fahleson, U.V., Bering, E.A., and Sheldon, W.R., 1980: Trigger, An Active Release Experiment that Stimulated Auroral Particle Precipitation and Wave Emissions, J. Geophys. Res., 85, 5043.

Holmgren, G., Marklund, G., Eliasson, L., Søraas, F., Opgenoorth, H., Primdahl, F., Haerendel, G., and Kintner, P.M., 1986: Ionospheric Response to Chemical Releases in the High-Latitude E and F regions, Proceedings of the Conference on Active Experiments, 30 June - 3 July, 1986, Toulouse, France.

Jones, R.A. and Rees, M.H., 1972: Time Dependent Studies of the Aurora-1. Ion Density and Composition, Planet. Space Sci. 21, 537.

Kelley, M.C., Fahleson, U.V., Holmgren, G., Boström, R., Kintner, P.M., and Kudeki, E., 1980: Generation and Propagation of an Electromagnetic Pulse in the Trigger Experiment and Its Possible Role in Particle Acceleration, J. Geophys. Res., 85, 5055.

Landau, L.D. and Lifshitz, E.M., 1959, Fluid Mechanics, Vol.6 in Course of Theroetical Physics, Pergamon Press.

Lundin, R. and Holmgren, G., 1980: Rocket Observations of Stimulated Electron Acceleration Associated with the Trigger Experiment, J. Geophys. Res., 85, 5061.

Mallincrodt, A.J. and Carlson, C.W., 1978: Relations Between Transverse Electric Fields and Field-Aligned Currents, J. Geophys. Res., 83, 1426.

Marklund, G., Raadu, M.A., and Lindqvist, P.-A., 1985: Effects of Birkeland Current Limitation on High-Latitude Convection Patterns, J. Geophys. Res., 90, 10864.

Rees, M. and Walker, J.C.G., 1968: Ann. Geophys. 24, 193.

Appendix 1

Description of the chemical composition of the cloud

In the TOR and Trigger experiments a TNT-Al-$CsNO_3$ mixture was used for the explosive charge. The weight proportions for the TOR experiment was : 50% TNT, 37.5% $CsNO_3$ and 12.5% Al (private communication with Dr H. Föppl). For the Trigger experiment the weight proportions between $CsNO_3$ and Al are 2.7:1, i.e. similar to TOR, but the TNT content is for Trigger somewhat uncertain. The major reaction products are CO, H_2, C, Cs or CsO_2H_2 and Al or condensed Al_2O_3. The energy content of the mixture is 4200 kJ/kg. Due to the low ionization potential of Cs (3.87 eV) as compared to the other gaseous products, Cesium will totally dominate the ion composition of the cloud. This is also verified by model calculations of the reaction products for an explosion of this kind as performed by the Swedish Research Institute for National Defense (Flygar, private communication). The calculations are made for three different cases corresponding to combustion under the assumptions of:
1) constant pressure, 2) constant temperature, 3) constant volume.

The degree of ionization of the Cesium turns out to be roughly 5×10^{-5} for the last two cases but very much higher (10^{-2}) for case 1. Radar reflections from ionized clouds have indicated that the degree of ionization of the Cesium is 1.6×10^{-3} when the initial expansions has been completed, according to Rosenberg and Golomb (1963). The neutral Cesium number density is typically 4.5 - 5% of the reaction products for the kind of mixture used in the TOR experiment. This is somewhat lower than the estimate of 6% for the kind of mixture used in the Trigger experiment, as given by Rosenberg and Golomb (1963). They also estimate that 2.5×10^{26} gaseous molecules are liberated from 18 kg of this TNT-Al-$CsNO_3$ mixture. For Trigger the 12 kg mixture would thus correspond to 1.7×10^{26} liberated molecules and for TOR the 10 kg mixture would correspond to 1.4×10^{26} liberated molecules.

The ambient plasma at 170 km altitude is dominated by the ion species: NO^+, O_2^+ and O^+ and the neutral species: N_2, O_2 and O (Jones and Rees, 1972).

As discussed in Section 5, the particle layer just behind the shock front is not dominated by cloud plasma but swept-up ambient plasma. From this region towards the center of the explosion there will be a change in the chemical composition from that of the ambient plasma to that of the cloud. Let us summarize by listing some of the relevant parameters that can be calculated using the above information and that will be used in the model calculations.

<u>Cloud plasma:</u>

$\langle m_i \rangle \approx 133$ m.u.

$\langle m_n \rangle \approx 24$ m.u.

$N_n(\text{TOR}) \approx 1.4 \times 10^{26}$ particles

N_n (Trigger) $= 1.7 \times 10^{26}$ particles

$N_{cs}/N_n \approx 4.7\%$

<u>Ambient plasma:</u>

$\langle m_i \rangle \approx 30$ m.u.

$\langle m_n \rangle \approx 25$ m.u.

$n_n(164\text{-}170 \text{ km}) = 2.4\text{-}3 \cdot 10^{16}$ [m^{-3}]

(from Jones and Rees, 1972)

Appendix 2

Relation between j_φ and E_φ

Let the azimuthal current flow in a cylindrical shell section with uniform current density, a radial width D and a thickness (height) L. Also let this shell section follow the neutral gas in the expansion. From this a relation between the azimuthal (induced) electric field $E_\varphi(r)$ and the azimuthal current j_φ (centered at the radius r_o) as defined by Eq.(3) above, can be derived

From

$$\oint B \cdot ds = \mu_o I_\varphi \tag{34}$$

we obtain

$$j_\varphi = \frac{1}{\mu_o D} \Delta B \tag{35}$$

From

$$\oint E \cdot ds = -\frac{d\Phi}{dt} \tag{36}$$

we obtain

$$E\varphi \cdot 2\pi r = -\, 2\pi r_o \Delta B \cdot V \tag{37}$$

where $V = r_o/t$

Combining Eq.(35) and Eq.(37) we obtain

$$j\varphi = -\,\frac{r}{r_o}\;\frac{1}{\mu_o D V}\,E\varphi \tag{38}$$

By equating the two expressions for $j\varphi$ (Eqs.(3) and (38)) $E\varphi$ can be solved for as a function of E_r: E_φ is found to be smaller than both E_r and $V_n B$ by the factor R_m. Inserting this expression of E_φ into Eqs.(2) and (3) we finally obtain:

$$j_r = \sigma_P E_r \left(1 + \left(\frac{\sigma_H}{\sigma_P}\right)^2 / (1 + R_m^{-1})\right) + \sigma_H v_n B (1 + R_m)^{-1} \quad (39)$$

$$j_\varphi = -\sigma_H E_r \, (1 + R_m)^{-1} + \sigma_P v_n B (1 + R_m)^{-1} \quad (40)$$

$$\text{where } R_m = \frac{r_o}{r} \mu_o D V \sigma_P \quad (41)$$

For typical values: $D \leq 200m$; $\sigma_P \leq 10^{-3}$ S/m; $v \leq 4$ km/s; $\mu_o = 4\pi \cdot 10^{-7}$; $r_o \approx r$, R_m becomes typically less than 10^{-3}. For $R_m << 1$ the expressions for j_r and j_φ reduce to Eqs.(4) and (5) given above. This also justifies the assumption of essentially unchanged magnetic field at r_o made in Section 4 above.

Appendix 3

Estimate of Σ_A/Σ_P

Σ_A defined on page 8 can be rewritten as:

$$\Sigma_A = \left(\frac{m_i^a \, n_i^a}{\mu_o}\right)^{1/2} / B \qquad (42)$$

where m_i^a, n_i^a here represents the mass and density of the ambient ions.

The Pedersen conductivity is given by

$$\sigma_P = \frac{\omega_{ci}/\nu_{in}}{1+(\omega_{ci}/\nu_{in})^2} \cdot \frac{e \, n_i^c}{B} \qquad (43)$$

where ω_{ci} and ν_{in} are given by Eqs.(20) and (19) above and n_i^c represents the ion density in the cloud. At the time when the peak field is observed $\omega_{ci}/\nu_{in} \approx 1$ which gives

$$\sigma_P \approx \frac{1}{2} \frac{en_i^c}{B} \qquad (44)$$

For the cylindrical symmetry assumed, the heightintegrated Pedersen conductivity is simply given by:

$$\Sigma_P \approx \Delta H \cdot \frac{1}{2} \frac{en_i^c}{B} \qquad (45)$$

where $\Delta H \approx \sqrt{\pi} \, V_{ex} \cdot t^o$ at the time of the peak in the electric field (cf. Fig.4).

The ion densities n_i^a and n_i^c needed to calculate Σ_A and Σ_P can be estimated from the plasma density observations on TOR and Trigger as summarized in Table 3, and from the geometry of the experiments illustrated in Figs. 1 and 4.

We want to calculate n_i^c at the radial distance r_o from the the cloud center at the point denoted by · (cf. Fig. 4). This is where the electric field pulse is assumed to originate. The mapping factors between n_i^c (r_o) and the peak densities measured on the rocket n_i^{max} are given below for two different assumptions concerning the form of the ion expansion.

I. Spherical expansion (SE)

$$n_i^c (r_o) \approx (\frac{d}{r_o})^3 n_i^{max} \tag{46}$$

where d = 1.2 km i.e. the distance between the rocket and the cloud center.

II. Cylindrical expansion (CE)

(Transverse expansion blocked)

$$n_i^c (r_o) \approx \frac{d}{r_o} \cdot n_i^{max} \tag{47}$$

The estimates of Σ_A/Σ_P and the corresponding reduction factor β for the two different rockets and the two different cases described by Eqs. (46) and (47) are presented in Table 2.

Release experiment	n_n-model	$r_s(t^m)$[m]	r_o [m]	$n_n(r_o)$ [m^{-3}]	$V_n(r_o)$ [m/s]	$n_n(r_o)\cdot V_n(r_o)$ [$m^{-2}\cdot s^{-1}$]
TOR	1.freely expand. cloud	682	590	$4.7\cdot10^{16}$	$9.8\cdot10^{3}$	$4.6\cdot10^{20}$
Trigger	- " -	852	730	$3.0\cdot10^{16}$	$6.9\cdot10^{3}$	$2.1\cdot10^{20}$
TOR	2. shock model	682	590	$1.2\cdot10^{17}$	$3.6\cdot10^{3}$	$4.4\cdot10^{20}$
TRIGGER	- " -	852	730	$1.5\cdot10^{17}$	$2.6\cdot10^{3}$	$3.90\cdot10^{20}$
COMMENTS	discussed in Sect.5	radius of shock front at time of E_{max} Eq.(26)	calcul. from the geometry of the experim. cf.Fig.1	given by Eq.(1) (free expansion) or Eq.(28) (shock)	given by Eq.(21)(free expansion) or Eq.(27) (shock)	

Table 1. Comparison of the calculated momentum, $n_n v_n$ in an expanding cloud using 1. a free expansion model 2. a shock model.

Model profile no	σ (m^2)	V_{rel} (m/s)	t^o (ms)	r_o (m)	V_{ex} (m/s)	N_n	$\langle m_i \rangle$ (mu)	ω_{ci} (rad/s)
TOR I	$4.86 \cdot 10^{-19}$	$3.6 \cdot 10^3$	60	590	$6.95 \cdot 10^3$	$1.4 \cdot 10^{26}$	30	160
" II	$4.46 \cdot 10^{-19}$	$2.0 \cdot 10^3$	"	"	"	"	133	36
" III	"	$2.4 \cdot 10^3$	"	"	"	"	133	36
Trigger I	$4.86 \cdot 10^{-19}$	$2.6 \cdot 10^3$	105	730	$4.92 \cdot 10^3$	$1.7 \cdot 10^{26}$	30	160
" II	$4.46 \cdot 10^{-19}$	$1.4 \cdot 10^3$	"	"	"	"	133	36
" III	"	$2.4 \cdot 10^3$	"	"	"	"	133	36
	For explanation see text	given by the typical v_n values in the three regions	given by the time for the observed E_{max}	given by the geometry of the experiment cf.Fig.1	obtained from r_o and t^o using Eq.(24)	given by the details of the explosive and of the ambient plasma (cf. Appendix 1)		

Table 2. Input parameters to the model profiles of the electric field.

	TOR		TRIGGER	
	SE	CE	SE	CE
n_i^a [m^{-3}]	$2 \cdot 10^{10}$		$1.5 \cdot 10^{10}$	
n_i^{max}[m^{-3}]	$2.5 \cdot 10^{11}$		$2.5 \cdot 10^{11}$	
$(d/r_o)_{CE}$		2		3.33
$(d/r_o)^3_{SE}$	8		7	2
$n_i^c(r_o)$[m^{-3}]	$2 \cdot 10^{12}$	$5 \cdot 10^{11}$	$9.2 \cdot 10^{12}$	$8.3 \cdot 10^{11}$
$\Sigma_P(S)$	2.4	0.60	26	0.73
$\Sigma_A(S)$	0.55	0.55	0.48	0.48
Σ_A/Σ_P	0.23	0.92	0.18	0.66
$\beta=(1+\frac{2\Sigma_A}{\Sigma_P})^{-1}$	0.68	0.35	0.74	0.43

Table 3. Estimate of Σ_A/Σ_P and the reduction factor β from the ion density measurements made on the rockets. n_i^a, represents the ambient density before and well after the explosion; n_i^{max}, the peak ion density measured shortly after the explosion; $n_i^c(r_o)$, the estimated ion density mapped from the rocket along $\underline{B}$ to a closet distance r_o from the cloud center using the mapping factors (d/r_o) and $(d/r_o)^3$ defined by Eqs. (37) and (38). Σ_A is the Alfvén wave conductance and Σ_P the heightintegrated Pedersen conductivity inside the cloud calculated from Eqs. (33) and (36).

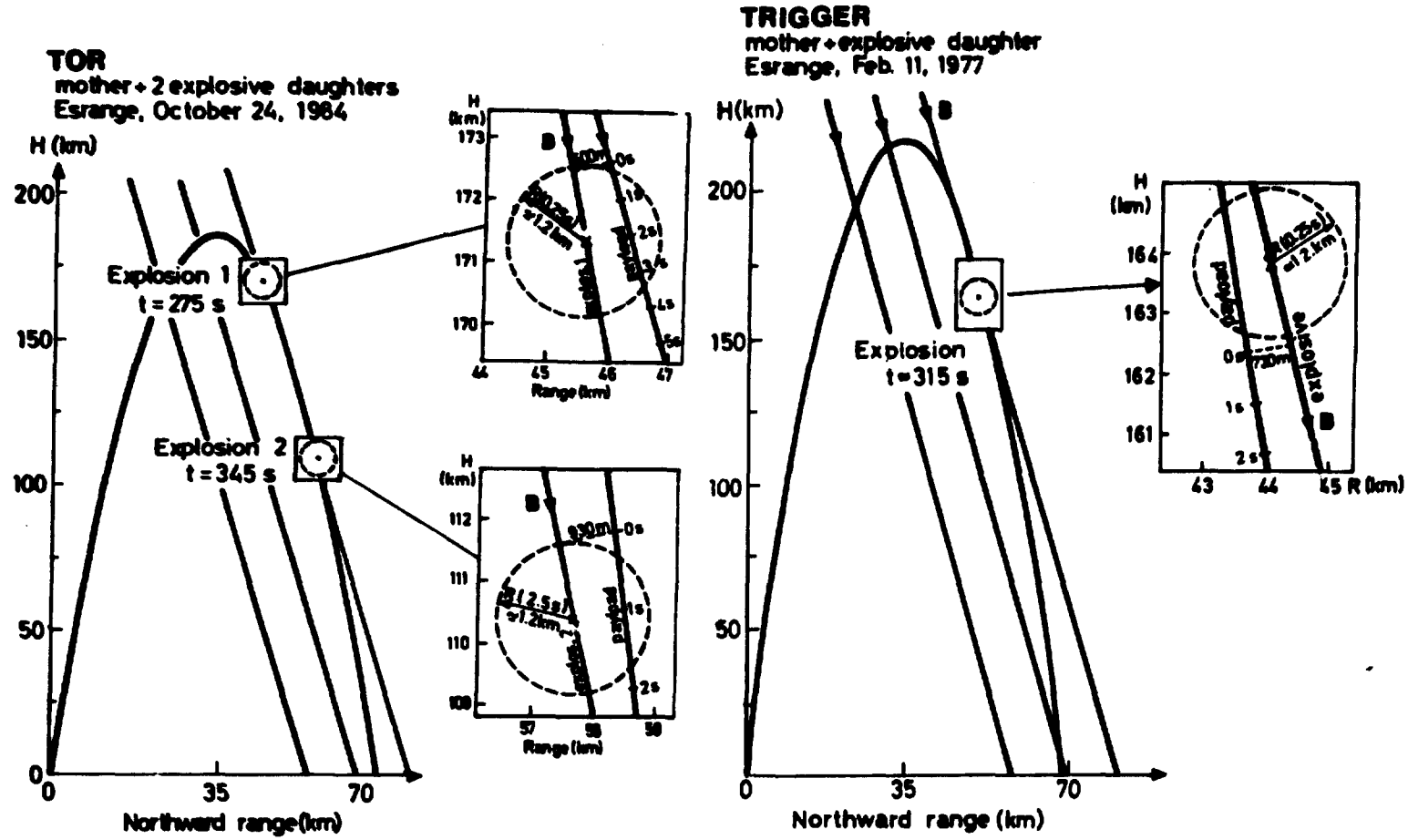

Fig. 1 Trajectory plots for the TOR and Trigger release experiments. The upper part of the downleg trajectories where the releases take place almost perfectly traces the magnetic field. The inserts show in more detail the geometric relationship between the cloud and the payload trajectory around the explosion time.

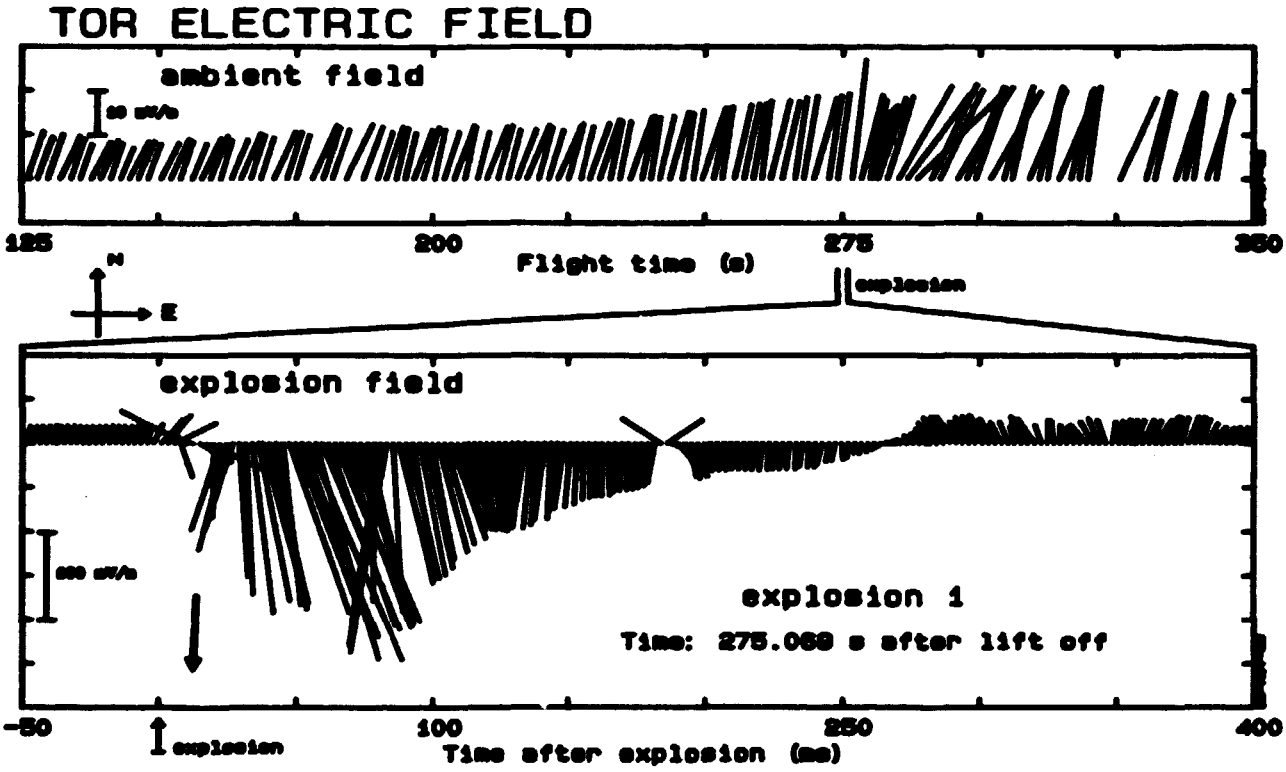

Fig. 2 Vector plot of the horizonthal electric field observed on the TOR rocket, launched from Esrange on October 24, 1984.

Upper panel: Background ionospheric electric field vs flight time (s). The thick arrow represent the electric field vector deduced from the STARE-drift data.

Lower panel: Electric field associated with the release vs time after the explosion (ms). The thick arrow represent the direction towards the cloud centre.

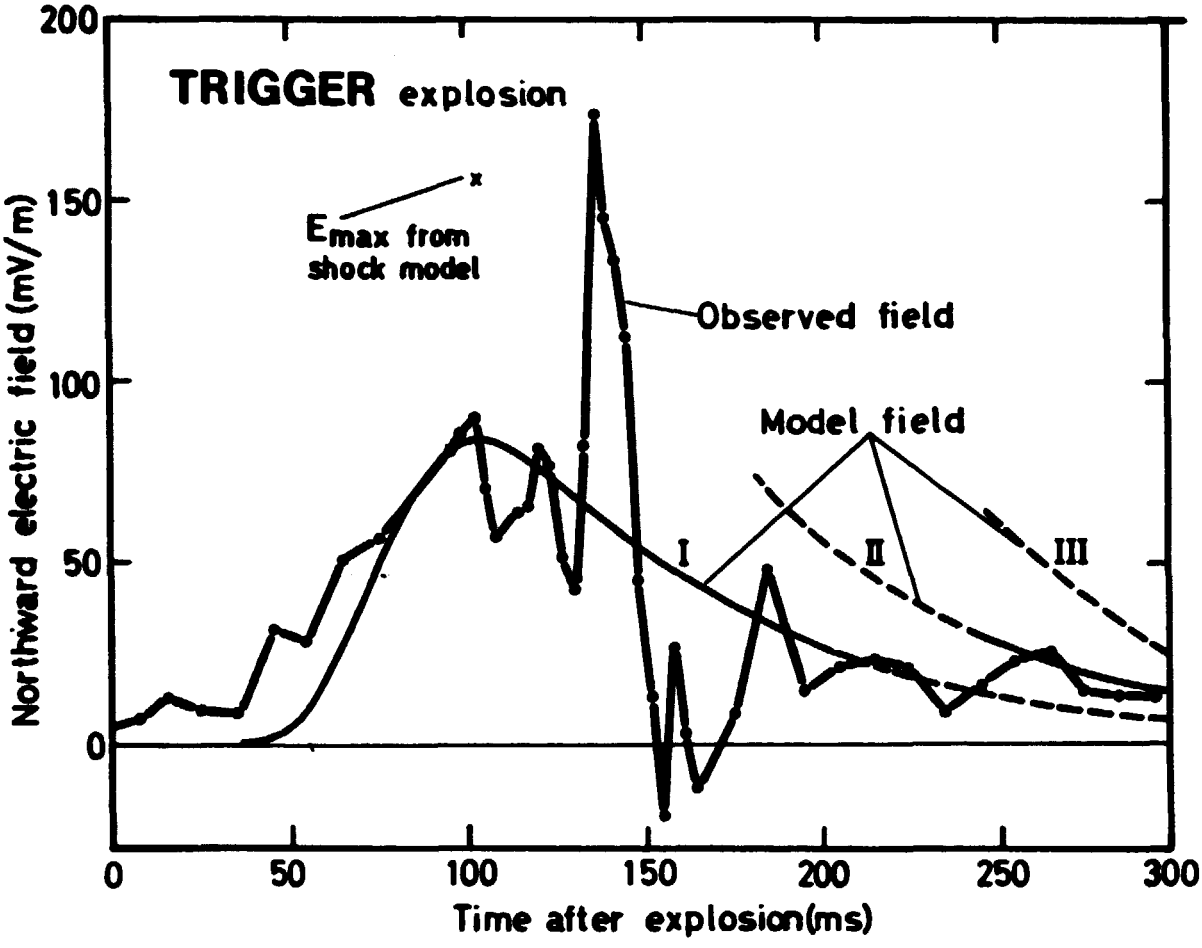

Fig. 3 Time profiles of the northward component of the electric field associated with the Trigger release.
The model fields labelled I, II, and II correspond to the different regions of the cloud as demonstrated in Fig.6. Profile 1 corresponds to the central part of the puls, with a layer of swept up ambient particles behind the shock front. The cross represents the electric field maximum obtained from the shock model for the ideal case with no damping of the particle density behind the front.

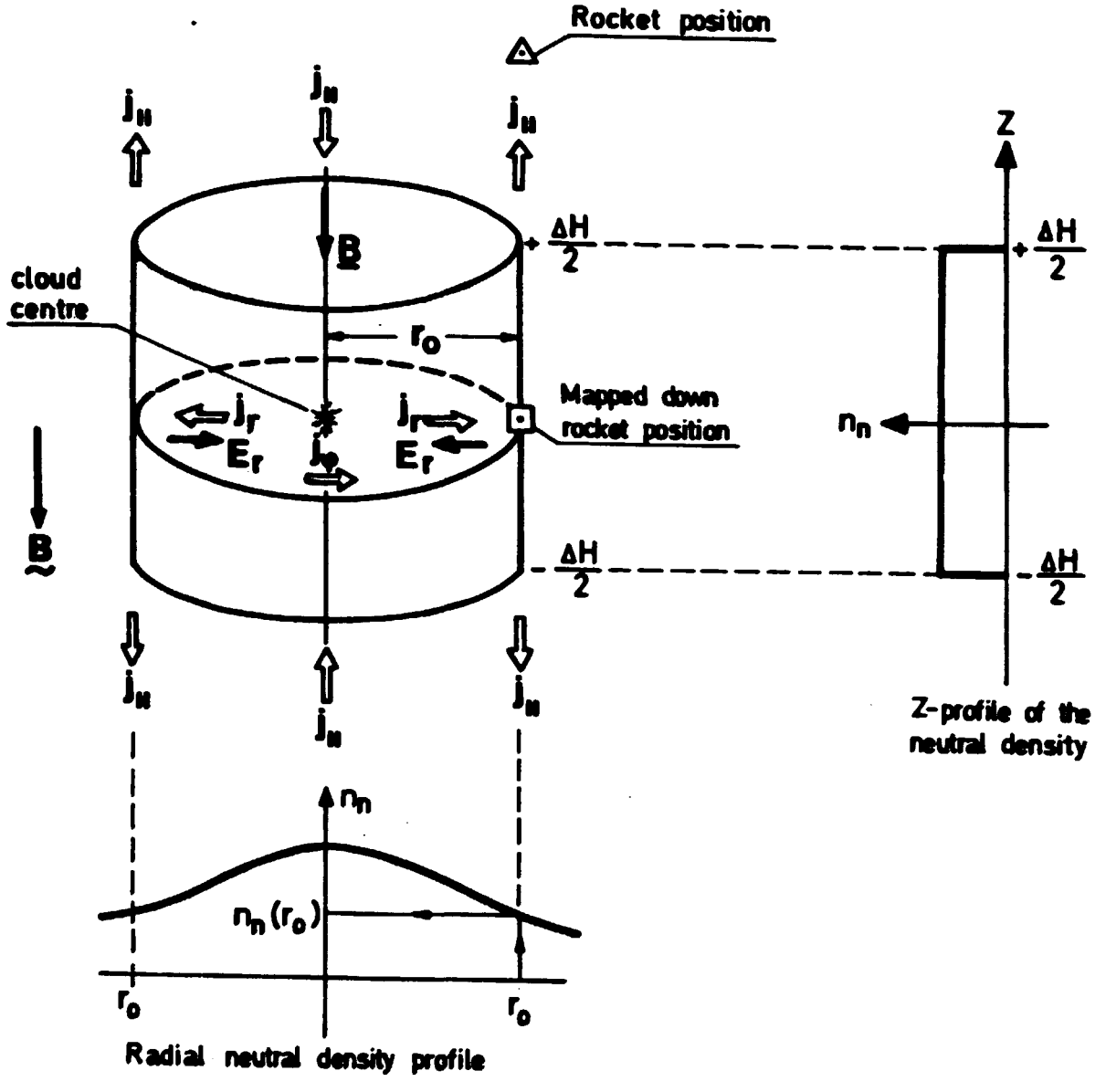

Fig. 4 Description of the cloud model.
The neutral density profiles in the radial and Z-direction, as assumed in the model, are shown by the two schematic graphs. The model simulates the time profile of the electric field at the mapped down rocket position denoted by △ at the radial distance r_o. The cloud constitutes a localized ionospheric generator, E_r, driving a generator current j_r which is closed by field-aligned currents $j_\parallel$.

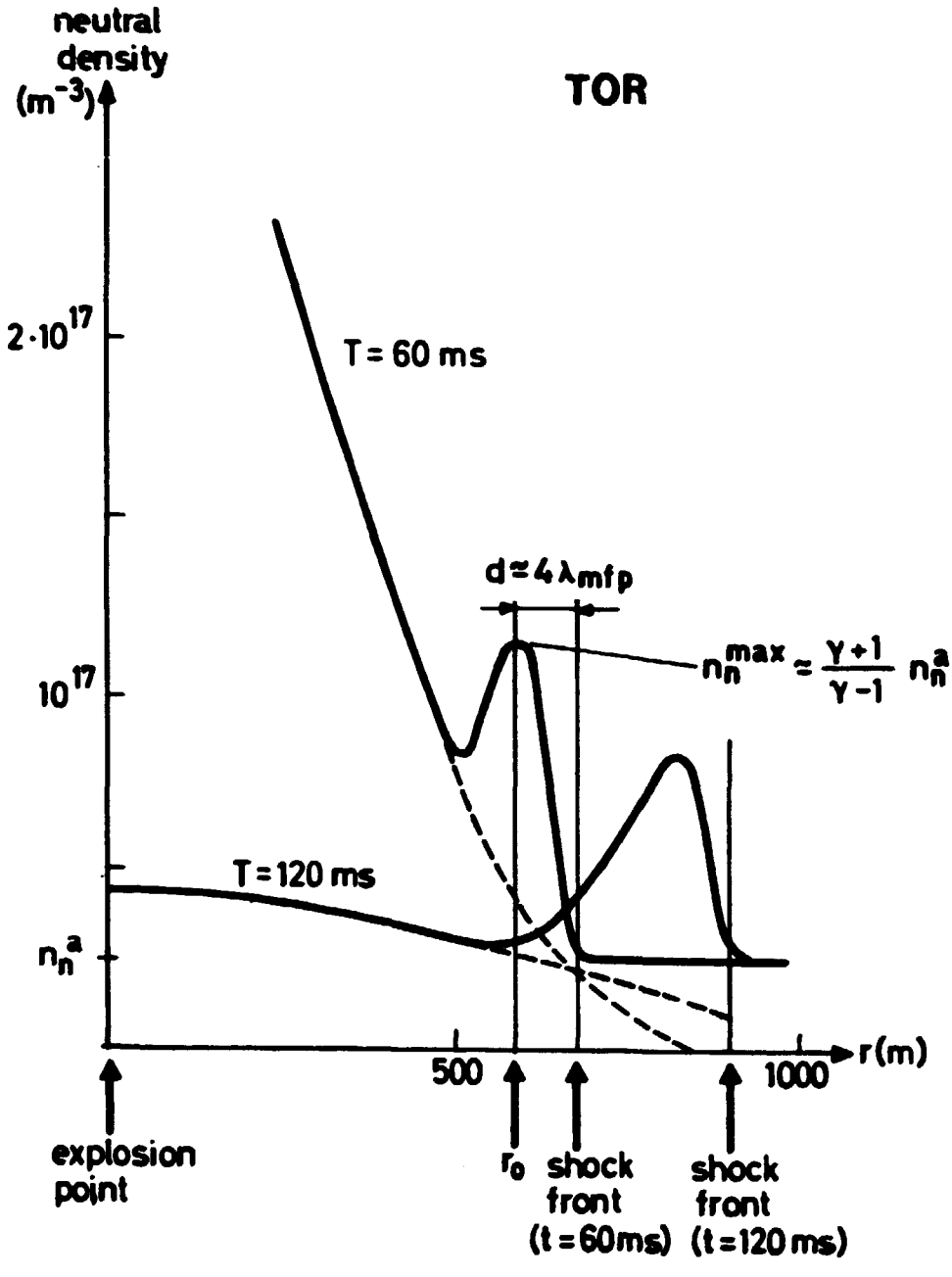

Fig. 5 Refined picture of the neutral density profile presented in Fig. 4. In addition to the Gaussian distribution in the central parts of the cloud, here represented by solid lines for r < 500 m and dashed lines for r > 500 m we have schematically added the density peak associated with the shock. n_n^{max} is for the ideal case five times larger ($\langle\gamma\rangle \approx 1.5$) than the ambient density, n_n^a. At T = 60 ms, the density in the central part of the cloud is still relatively high, the density peak a few λ_{mfp} behind the shock has reached r_o and the rocket (connected with r_o) measures the intense electric field peak. At T = 120 ms the central density has decreased almost to the ambient value, as has the particle density at r_o.

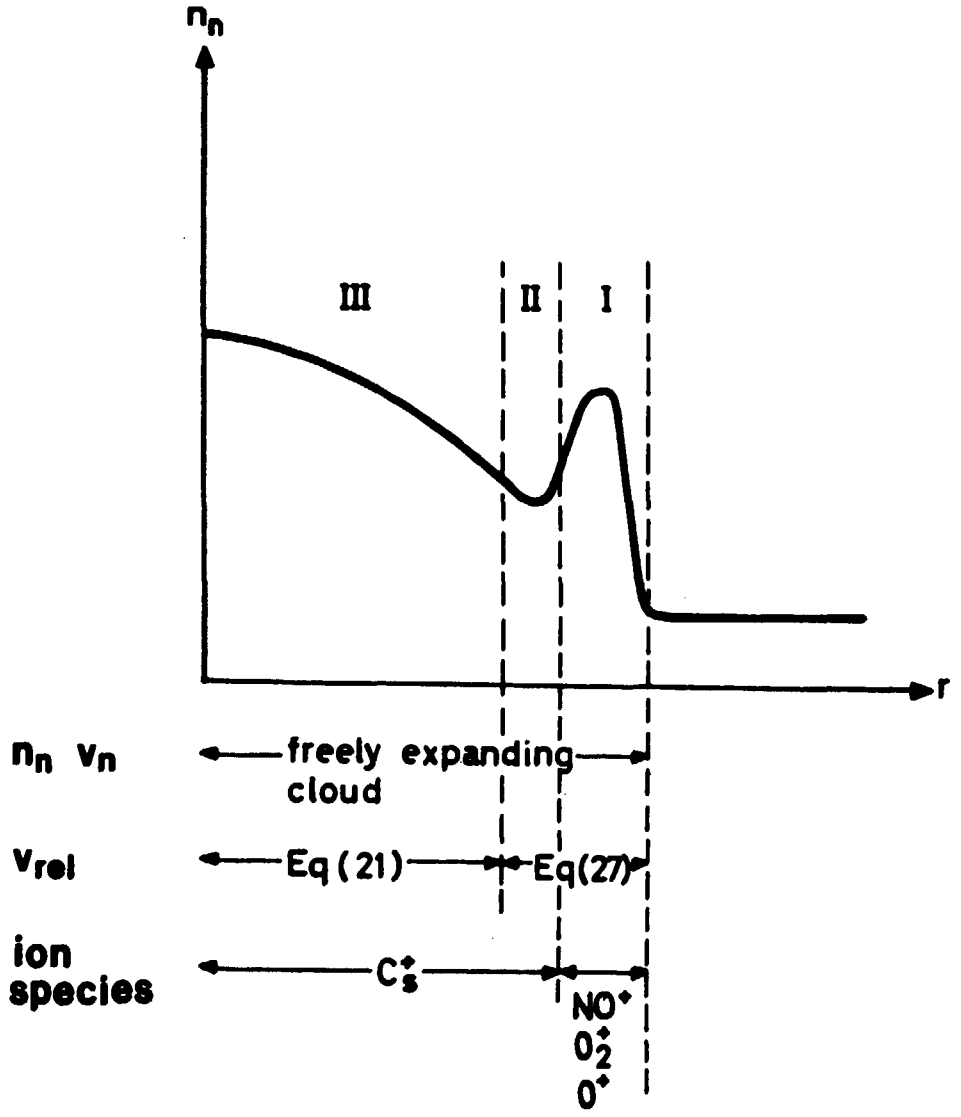

Fig.6 Schematic picture of the radial density profile through the cloud. Region I represents the shock-dominated region; Region III, that of the freely expanding cloud and Region II an intermediate region. As explained in the text the product $n_n v_n$ is well described by the free expansion throughout the cloud (although n_n and v_n separately are not). The regions correspond to different models of $n_n v_n$, v_{rel} and the ion species to use in Eq.(25).

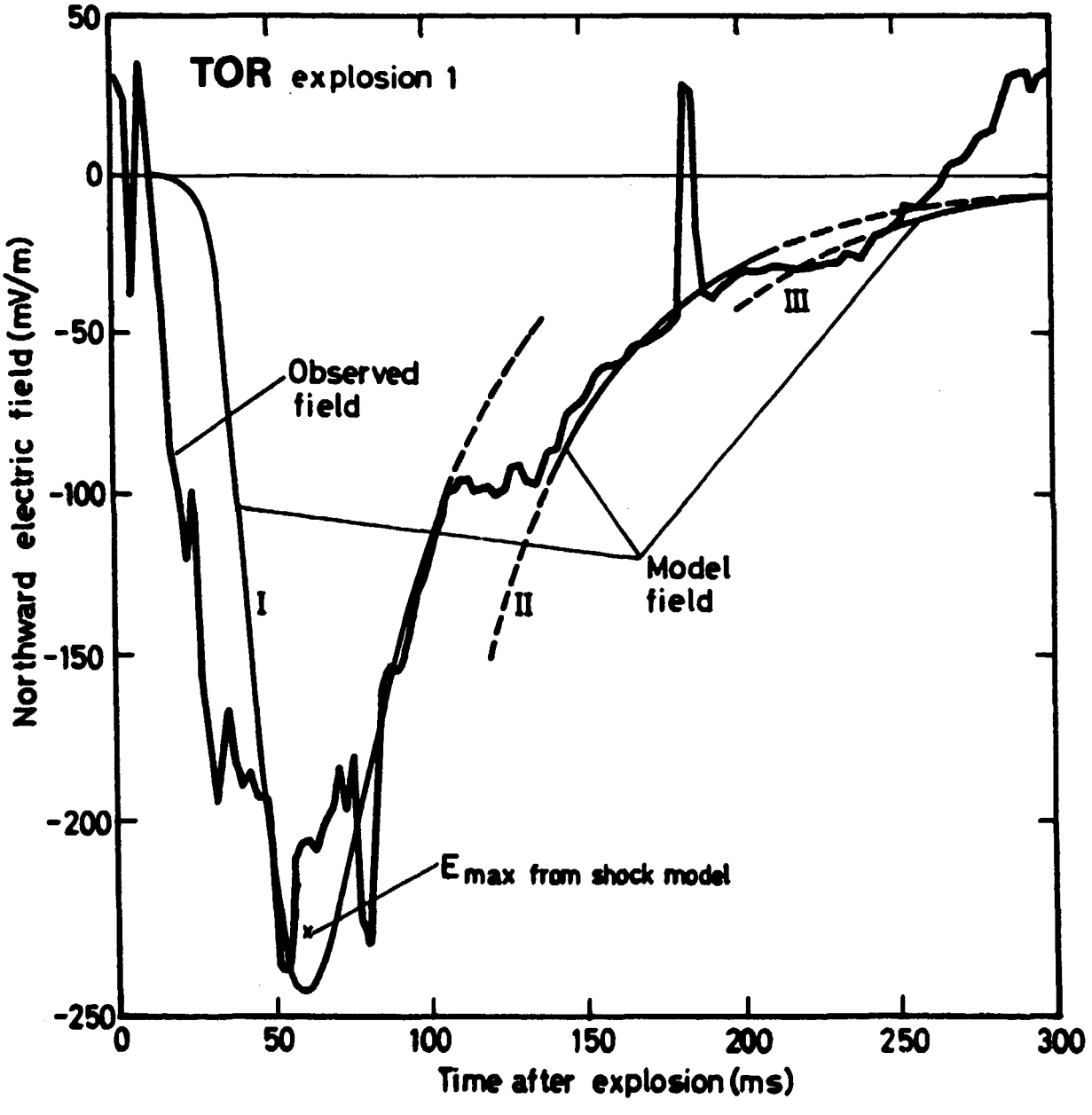

Fig. 7 Time profiles of the southward component of the electric field associated with the TOR release (for explanation, see Fig.3). Note the excellent agreement in magnitude and general shape between the model results and the observation.

TRITA-EPP-86-01 ISSN 0348-7539

The Royal Institute of Technology, Department of Plasma Physics
S-100 44 Stockholm, Sweden

ON TRANSIENT ELECTRIC FIELDS OBSERVED IN CHEMICAL RELEASE EXPERIMENTS BY ROCKETS

G. Marklund, N. Brenning, G. Holmgren, and G. Haerendel
June 1986, 38 pp. incl. illus., in English

As a follow-up to the successful chemical release experiment Trigger in 1977, the TOR (Trigger Optimized Repetition) rocket was launched from Esrange on Oct. 24, 1984. Like in the Trigger experiment a large amplitude electric field pulse of 200 mV/m was detected shortly after the explosion. The central part of the pulse was found to be clearly correlated with an intense layer of swept up ambient particles behind a propagating shockfront. The field was directed towards the centre of the expanding ionized cloud, which is indicative of a polarisation electric field source. Expressions for this radial polarisation field and the much weaker azimuthal induced electric field are derived from a simple cylindrical model for the field and the expanding neutral cloud. Time profiles of the radial electric field are shown to be in good agreement with observations.

Key words: Electric fields, Polarisation electric fields, Birkeland currents, Shock wave propagation, Rocket experiments, Auroral arcs.